

# Spectroscopic and photometric time series of the bright RRc star T Sex

József M. Benkő<sup>1,2\*</sup>, Ádám Sódor<sup>1,2</sup> and András Pál<sup>1</sup>

<sup>1</sup>*Konkoly Observatory, Research Centre for Astronomy and Earth Sciences, Konkoly Thege M. u. 15-17., H-1121 Budapest, Hungary*

<sup>2</sup>*MTA CSFK Lendület Near-Field Cosmology Research Group*

Accepted 2020 October 30. Received 2020 October 30; in original form 2020 September 24

## ABSTRACT

We present spectroscopic time series observations on one of the brightest northern RRc star, T Sex. Additionally, we also analysed extended photometric data sets, particularly the recent observations of the *TESS* space telescope. The main findings of our studies are as follows: T Sex, unlike all RRc stars whose space photometry has been analysed, shows only the  $0.5f_x$  frequency as an additional pulsation frequency. With this, T Sex may be the first represent of such rare RRc stars found from space photometry. The spectroscopic data show a periodic distortion of the H $\alpha$  line with the pulsation phase. This phenomenon has not been reported for any RR Lyrae stars. The characteristic line distortion is probably caused by the turbulent convection, which resulted in higher macroturbulent velocity for T Sex than for typical RRab stars. Line doubling of the Na D line was observed between the 0.37 and 0.80 pulsation phases. The explanation of this phenomenon is that the two absorption components originate from different sources. The redder component comes from the pulsating atmosphere of the star, while the bluer one from the interstellar space. At phase 0.438, we detected emission on the Na D line, which may indicate a weak shock wave.

**Key words:** stars: oscillations – stars: variables: RR Lyrae – stars: individual: T Sex – methods: data analysis – space vehicles

## 1 INTRODUCTION

Variable stars are typically investigated by photometric time series. Spectroscopic and, in particular, spectroscopic time series analyses are less frequent. It has practical reasons; spectroscopy is generally a more “expensive genre”. For a given star, spectroscopy requires a larger telescope, more complex and more expensive equipment than photometry. This general difficulty is even more serious for RR Lyrae stars because their relatively faint apparent magnitudes ( $m_v > 7.45$  mag), short periods (0.3–0.7 d) and non-sinusoidal light variations limit the feasible integration time. The actual situation was well described by Jurcsik et al. (2017): “Complete radial velocity curves were published for less than 50 Galactic field RR Lyrae stars and less than 10 RR Lyraes in globular clusters previously.” The circumstances, however, are gradually changing as modern echelle spectrographs become more and more prevalent. These powerful tools provide useful data on RR Lyrae stars even with relatively small telescopes. This is demonstrated nicely by some recent spectroscopic time series studies (e.g. Chadid et al. 2017; Sneden et al. 2017; Gillet et al. 2019).

Spectroscopic time series studies of RRc stars – RR Lyrae pulsating in their first overtone mode – are even less frequent than studies of fundamental-mode pulsator RRab stars, though RRc stars

are by no means less interesting objects. Olech & Moskalik (2009) reported a new class of double pulsating RR Lyrae stars when they discovered two RRc stars in the globular cluster  $\omega$  Cen which pulsate with an additional mode beyond their dominant radial first overtone mode. This surprising new phenomenon has been identified in all RRc stars by analysing *Kepler* and *CoRoT* space photometric data (Moskalik 2013; Moskalik et al. 2015; Szabó et al. 2014; Sódor et al. 2017). The period ratio of these additional modes with the dominant (overtone) one  $P_x/P_1$  are always in a narrow range around 0.61 or 0.63. Soon, further additional modes were also found in ground-based observations of some RRc stars at period ratios of 0.68 (Netzel et al. 2015) and 0.72 (Prudil et al. 2017). On the basis of his simplified model calculations, Dziembowski (2016) suggested that the additional frequencies of the first two groups ( $P_x/P_1 \sim 0.61$ ,  $P_x/P_1 \sim 0.63$ ) might be associated with  $l = 8$  or  $l = 9$  non-radial modes. The nature of the other two groups are still mysterious. We have to stress that such kind of additional modes have never been detected in any of the RRab stars. Additional modes were also discovered in RRab stars, but at different period ratios, and those have different explanations. The additional modes of RRc stars appear in classical double mode (RRd) stars as well. In fact, the first space observation for such modes occurred in the RRd star AQ Leo (Gruberbauer et al. 2007). An overtone pulsation appears to be necessary for the excitation of these modes.

These new phenomena have drawn our attention to RRc stars.

\* E-mail: benko@konkoly.hu

**Table 1.** Log of T Sex spectroscopic observations

Night (yyyy-mm-dd)	JD (-2 400 000)	$\langle S/N \rangle$	$\phi$	$n$
2015-03-05	57087	11	0.606-0.732	2
2015-03-07	57089	51	0.003-0.932	14
2015-03-10	57092	19	0.020-0.945	7

Since space photometric results suggested that each RRc star shows extra modes, the target selection appeared to be an easy task. According to Maintz (2005), only six RRc stars brighter than ten visual apparent magnitude are known in the northern sky. The brightest one (V764 Mon,  $V_{\max} = 7.13$  mag,  $P_1 = 0.29$  d) is even brighter than RR Lyr itself. Therefore, we focused on this star but we also selected another, slightly fainter object, T Sex ( $V_{\max} = 9.81$  mag,  $P_1 = 0.3247$  d) as secondary target in the observing window of V764 Mon. We sought to achieve the most complete pulsation-phase coverage with the shortest possible integration times for both stars.

A quick look at the spectra revealed that V764 Mon is not, in fact, an RR Lyae, but a fast-rotating  $\delta$  Scuti star. The results about this star will be published elsewhere. In this paper, we study T Sex, a bona fide RRc pulsator.

## 2 OBSERVATIONS AND REDUCTION

### 2.1 Photometric data

Two sufficiently extensive photometric time series were analysed. The ASAS-3 V band data (All Sky Automated Survey, Pojmański et al. 2005) contains 504 observed data points. Before the analysis, the outlying points fainter than 10.4 mag and the less accurate observations flagged by ‘D’ in the data base had been removed. In the end, 457 data points remained.

Up to the time of writing of this manuscript, the *TESS* space mission (Ricker et al. 2015) observed T Sex once, in Sector 8, obtaining 17 755 data points. The observation of Sector 8 was taken in February 2019 almost continuously, covering 24.62 days with 2 min exposures. This exposure time represents oversampled high-cadence observations<sup>1</sup>.

From the data offered by the archive, the light curves obtained from the corrected aperture photometry (PDCSAP) fluxes were used for this analysis, and only the best-quality data (marked with a quality flag 0) were used, which corresponds to 13 395 data points. The fluxes were transformed to a magnitude scale. We mention that *TESS* magnitudes (zero point, the amplitude and the errors) are scaled with the reference magnitude. We accepted the value of  $m_{\text{TESS}} = 9.779$  mag according to the *TESS* data release. The typical error of the individual photometric data points is  $\sim 0.0013$  mag.

### 2.2 Spectroscopic data

For the observations we used the ACE fibre-fed échelle spectrograph attached to the 1-m RCC telescope at the Piszkéstető mountain station of the Konkoly Observatory. The spectra cover the 4150–9150 Å wavelength range with a resolution of  $R \approx 20\,000$ . A total

<sup>1</sup> The data are publicly available at the Mikulski Archive for Space Telescopes: <https://mast.stsci.edu/portal/Mashup/Clients/Mast/Portal.html>

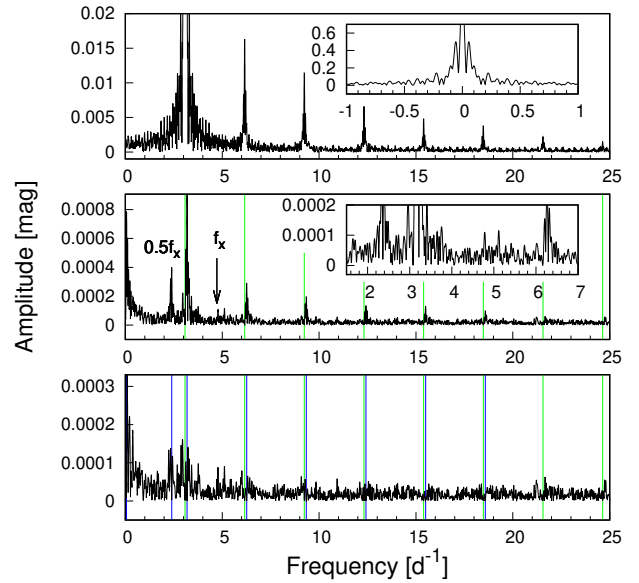


**Figure 1.** Fourier spectra of the *TESS* data on T Sex during the subsequent pre-whitening steps. Top panel: The original spectrum and the central part of the window function (inset). Middle panel: the spectrum after pre-whitening the data with the main pulsation frequency  $f_1$  and its 16 harmonics. Thin green vertical lines show the position of the pre-whitened frequencies. The inset in the middle panel is the expansion of the frequency range around  $0.5f_x$  and  $f_x$ . Bottom panel: residual after pre-whitening the spectrum shown in the middle panel with eight further significant frequencies (indicated with blue vertical lines). To make the harmonic structure more apparent, the amplitude limit on the top panel is lower than the amplitude of the main frequency (0.08 mag).

of 23 spectra were recorded from the target star on three nights between 5 and 10 March 2015 (Table 1). The integration time was 30 min, which is a good trade off between getting enough pulsation phase resolution and reaching acceptable signal-to-noise ratio (see column 4 in Table 1 for nightly averaged  $S/N$  values estimated by *rSPEC* (Blanco-Cuaresma et al. 2014; Blanco-Cuaresma 2019)).

The ACE spectra were reduced using standard IRAF (Tody 1986, 1993) tasks including bias, dark and flat-field corrections, aperture extraction, and wavelength calibration using thorium-argon calibration images, taken after every third object frames. The normalisation, cosmic-ray filtering, order merging were performed by our PYTHON scripts (developed by ÁS). Each spectrum was also corrected to the barycentric frame.

## 3 ANALYSIS OF THE PHOTOMETRIC DATA

Although this work focuses on spectroscopic time series observations of T Sex, we also needed some photometric data for determining the proper period and phases. Furthermore, the analysis of the photometric data yielded an unexpected result, too.

The ASAS data set was analysed by the Fourier fitting tool of the PERIOD04 package (Lenz & Breger 2005). Since these data points spread over 9 years (3276 days between December 2000 and November 2009), the Nyquist frequency ( $\sim 0.24$  d<sup>-1</sup>) is significantly lower than the pulsation frequency ( $f_1 = 3.0798$  d<sup>-1</sup>), and the Fourier spectrum had to be calculated well above this limit frequency. Consequently, the resulting spectrum has a periodic structure. It contains the main frequency, its daily alias frequencies and the annual aliases

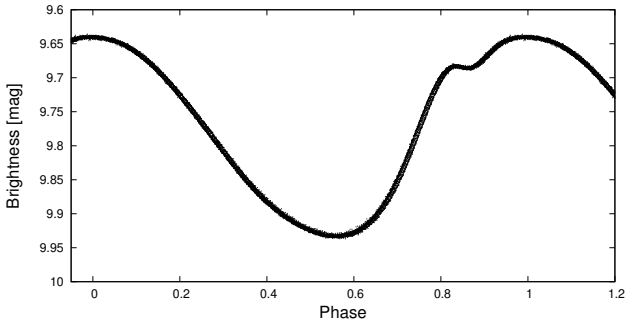


**Figure 2.** Phased light curve of T Sex observed by *TESS* satellite.

caused by the seasonality of the observations and the daily repetitions. The 1-year frequency also occurs in side peaks around the main frequency. Apart from the pulsation frequency, no additional frequency can be detected above the noise level ( $\sim 0.04$  mag).

The Fourier spectrum of the *TESS* data shows the main pulsation frequency ( $f_1 = 3.079 \text{ d}^{-1}$ ) and its harmonics (see top panel in Fig. 1). We pre-whitened the data with  $f_1$  and its all 16 significant harmonics up to the frequency  $50.0 \text{ d}^{-1}$ . The residual spectrum is shown in the middle panel of Fig. 1. Eight significant frequencies can be detected in this residual. Six of them can be written in the form  $k f_1 + f^{(1)}$ , where  $k = 1, 2, \dots, 6$ , and  $f^{(1)} = 0.103 \text{ d}^{-1}$ , moreover  $f^{(2)} = 0.055$  and  $f^{(3)} = 2.3919 \text{ d}^{-1}$ . All but one of these frequencies are of instrumental origin. The window function (inset in top panel of Fig. 1) contains the data length frequency ( $f^{(2)} = 0.055 \text{ d}^{-1}$ ). We can now identify  $f^{(1)} \approx 2f^{(2)}$ . These identifications are within the frequency errors because the short *TESS* data set the Rayleigh frequency resolution is rather low ( $0.04 \text{ d}^{-1}$ ).

The only significant ( $S/N = 5.7$ ) non-technical frequency is  $f^{(3)}$ . As mentioned in the introduction, all the space photometric measurements of RRc stars that have been studied show additional frequencies. The Fourier spectra of those stars typically contain a strong peak ( $f_x$ ) with a ratio to the main period  $f_1$  of around 0.61 or 0.63 (see blue squares in Fig. 3), as well as its harmonics and linear combinations with  $f_1$ , respectively. In some cases, the sub-harmonic  $0.5f_x$  is also detectable (*CoRoT* Szabó et al. 2014, *Kepler/K2* Moskalik et al. 2015; Molnár et al. 2015; Sódor et al. 2017).

One possible explanation for the missing  $f_x$  frequency of T Sex is that, as the above cited works have shown, the amplitude of  $f_x$  can change strongly over time. Perhaps *TESS* measured the star in a ‘low amplitude state’, when the amplitude of the frequency  $f_x$  was below the detection limit. We expect *TESS* to re-observe T Sex in February 2021 (Sector 35), and the question may be decided. However, Jurcsik et al. (2015), studying RRc stars of M3 by ground-based multicolour photometry, found that stars showing the  $f_x$  frequency are bluer than those not showing such a signal. This finding suggests intrinsic physical difference between these two groups of RRc stars.

According to Dziembowski (2016), signals at sub-harmonic frequencies  $0.5f_x$ , are the real frequencies of the non-radial modes of degrees  $l = 8$  and  $l = 9$ , and the signals at  $f_x$  are harmonics. Because of cancellation effects, the harmonic generally has better visibility than the mode frequency itself. On the large OGLE RRc sample, Netzel & Smolec (2019) showed recently that the longer-period sequence ( $P_x/P_1 \sim 0.63$ ) belongs most probably to the  $l = 8$  mode. Stars pulsating in this mode tend to show both  $f_x$  and  $0.5f_x$

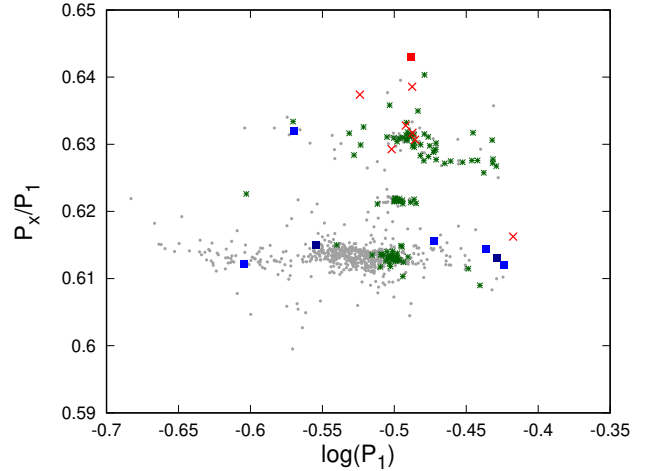


**Figure 3.** Petersen-type diagram of RRc stars showing the additional ( $f_x \sim 0.61$ ) frequencies. The OGLE RRc stars analysed by Netzel & Smolec (2019): grey dots are the  $RR_{0.61}$  sub-sample; green asterisks denote stars showing  $0.5f_x$  frequency as well, while red ‘x’ symbols show stars with  $0.5f_x$  without  $f_x$ . Filled squares indicate space results: light blue – *Kepler* (Moskalik et al. 2015; Sódor et al. 2017), dark blue – *CoRoT* (Szabó et al. 2014), red square – T Sex *TESS* (this work).

frequencies as well. From the 960 stars in which an additional mode was found by Netzel & Smolec (2019) (grey dots in Fig. 3),  $0.5f_x$  was also detected for 114 stars (green asterisks in Fig. 3) and even in 35 cases (3.6%), this frequency had larger amplitude than that of  $f_x$ . For another seven stars (red ‘x’-es in Fig. 3), only  $0.5f_x$  is detected.

If we identify  $f^{(3)}$  as  $0.5f_x$  then  $f_x = 4.7826 \text{ d}^{-1}$  and  $f_1/f_x = 0.643$  (see red filled square in Fig. 3). This ratio is higher than the median of the 0.63 sequence but within the observed range of this ratio. Such identification of  $f^{(3)}$  is likely because a peak, although not significant ( $S/N = 3.2$ ), is indeed visible at the position of the calculated  $f_x$  (see the inset in middle panel of Fig 1). Near to this one, at  $f^{(4)} = 5.1132 \text{ d}^{-1}$ , we can also see a peak of similar amplitude ( $S/N = 3.1$ ). The ratio of this frequency ( $f_1/f^{(4)} = 0.602$ ) suggests that it might be the harmonic of the  $l = 9$  mode. That is, T Sex contains both  $l = 8$  and  $l = 9$  mode pulsations as well. This is rather common phenomenon, Netzel & Smolec (2019) found this in more than 10% of their sample.

By removing the eight significant frequencies discussed above with a subsequent pre-whitening step, the residual spectrum shown in the bottom panel of Fig. 1 is obtained. No further significant ( $S/N > 4$ ) frequency can be detected in this spectrum but some low frequency excess can be seen. It has at least two sources: (i) a global instrumental trend and (ii) a cycle-to-cycle light curve variation similar to the found for RRab stars (see in Sec.4.1 in Benkő et al. 2019 for a discussion) since both phenomena are clearly visible in the *TESS* light curve of T Sex.

The pulsation period obtained from the *TESS* data ( $P_1 = 0.3248 \pm 0.004 \text{ d}$ ) is in agreement with the more precisely defined ASAS period ( $P_1 = 0.324696 \pm 0.00003 \text{ d}$ ). The *TESS* light curve folded with the ASAS period is shown in Fig. 2. Since the standard deviation of the curve is very small, no phase-shifted cycles are seen, it is likely that the period between the end of the ASAS measurements (2009) and the beginning of the *TESS* measurements (2019) did not change significantly.

**Table 2.** Sample of the radial velocity data tables. The columns contain the barycentric Julian date (BJD), the measured radial velocity  $v_{\text{rad}}$ , its uncertainty  $\sigma(v_{\text{rad}})$  and the corresponding pulsation phase  $\phi$ .

BJD (d)	$v_{\text{rad}}$ (km s $^{-1}$ )	$\sigma(v_{\text{rad}})$ (km s $^{-1}$ )	phase
2457089.25160	22.87	1.67	0.142584
2457089.27272	28.37	1.95	0.207629
2457089.29368	31.76	3.38	0.272182
2457089.32674	35.25	1.60	0.374000
2457089.34768	37.48	2.31	0.438491
(...)			

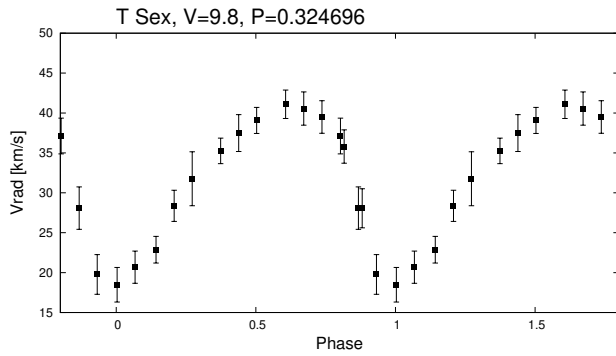


**Figure 4.** Radial velocity curve of T Sex. The error bars show the  $1\sigma$  calculated formal errors (around 1–2 km s $^{-1}$ ).

#### 4 RADIAL VELOCITY CURVE

We determined the radial velocity curve of T Sex. The radial velocities were calculated by cross-correlating the spectra with a metallic line mask containing 622 metallic lines between 4800 and 5600 Å. We used Gaussian fitting functions for determining the radial velocities and their uncertainties from the cross-correlation functions.

The S/N ratio in the cross-correlation functions are 80–150, which provide a precision of  $\sim 1$ –2 km s $^{-1}$  for the radial velocities. The systematic errors resulted in the data processing and the stability of the wavelength calibration system of the ACE instrument are better than 0.36 km s $^{-1}$ , based on observations of radial velocity standards (Derekas et al. 2017). The radial velocity curves are published as electronic tables. The structure of these tables is shown in the excerpt in Table 2.

We used here the ASAS-3 period determined above in Sec. 3. For zero phase of the radial velocity curve we simple used the current ephemeris of GEOS database<sup>2</sup> (Le Borgne et al. 2007) belonging to the photometric maxima because these two values are coincident within the observation error (Jurcsik et al. 2015, 2017; Sneden et al. 2017). The exact ephemeris was not critical in this study, but for the sake of completeness, we give it as we found from our polynomial fit:  $\phi_{v_{\text{rad}}}(0) = 2457089.529 \pm 0.08$ . The phase difference between radial velocity minimum and photometric brightness maximum in  $V$  is  $0.025 \pm 0.08$  in agreement with the previous study (Sneden et al. 2017). The obtained radial velocity phase curve in Fig. 4 demonstrates well the complete phase coverage of our observations.

Although T Sex is one of the brightest RRc stars, up to now only five radial velocity curves were published (Tift & Smith 1958; Preston & Paczyński 1964; Barnes et al. 1988; Liu & Janes 1989; Sneden et al. 2017) and phase coverage of these curves are complete only in Tift & Smith (1958), Barnes et al. (1988) and Liu & Janes (1989). By using the zero point of a four-element Fourier fit to the radial velocity curve we determined the mean velocity as  $v_0 = 31.7 \pm 0.5$  km s $^{-1}$ . This mean velocity is approximated the velocity of the stellar rest frame with respect to the solar system barycenter ( $v_\gamma$ ). Strictly speaking, however, this is not completely true, because the optical depth changes during the pulsation. The radial-velocity curve does not represent any physically moving fluid element (e.g. Karp 1975). However, the so-called k-term – the difference between  $v_\gamma$  and  $v_0$  – must be less than 2 km s $^{-1}$  for RRc stars. This value was found for more extended atmosphere of Cepheids by Nardetto et al. (2008).

Our mean velocity value is 6.5 km s $^{-1}$  higher than the latest published in the literature ( $v_0 = 25.2 \pm 1$  km s $^{-1}$ , Gontcharov 2006). This latter mean radial velocity compilation, however, is prepared for Galactic kinematic purposes and optimised for non-variable stars. As Kollmeier et al. (2013) showed, the mean radial velocity of RRc stars can be well estimated by measuring the radial velocity curve at the phase of  $\phi = 0.32$ . By a simple interpolation we obtain  $v(0.32) = 33.5 \pm 2.4$  km s $^{-1}$ . This value is consistent within  $1\sigma$  with our previous calculation and the recent measurements of Sneden et al. 2017. (They did not calculate  $v_\gamma$  for T Sex because of their incomplete phase coverage, but from their data we found  $v(0.32) = 28.6 \pm 2.5$  km s $^{-1}$ .)

### 5 SPECTRAL VARIATIONS WITH PULSATION PHASES

#### 5.1 Hydrogen H $\alpha$ line

Our spectra cover the hydrogen Balmer H $\alpha$ , H $\beta$  and H $\gamma$  lines. Since the detector is more sensitive in redder wavelengths, H $\alpha$  lines have the highest S/N ratio among the Balmer series. Therefore, we investigated the motions and line-profile variations of the H $\alpha$  line over the pulsation phase.

In Fig. 5, the H $\alpha$  line-profile variations of T Sex on the best night (2015-03-07) are plotted in the stellar rest frame. To make the phase dependence easier to follow, the normalised spectra are shifted vertically with phase dependent constants. The thin grey curves represent the original spectra. Since these spectra show many weak (mostly telluric) lines and some noise, we plot smoothed spectra as well (black curves in Fig. 5). The latter are better for following line profile variations.

If we look at the line positions, we find periodic shifts relative to the stellar rest frame: The H $\alpha$  line is blueshifted between phases  $\phi \sim 0.87$ –0.21 and redshifted between  $\phi \sim 0.37$ –0.74. This variation is the natural consequence of the radial pulsational motion in which the hydrogen-absorbing layer is involved and defines a radial velocity curve slightly different from the one obtained from metallic lines. These differences are discussed in detail by Sneden et al. (2017).

#### 5.2 Periodic line-profile distortions

The H $\alpha$  line, however, does not simply shift periodically around the laboratory wavelength corrected with the center-of-mass velocity, but its profile also changes with the pulsation phase. In Fig. 6, we show two highly asymmetric phases compared with a symmetric

<sup>2</sup> <http://rr-lyr.irap.omp.eu/dbrr/>

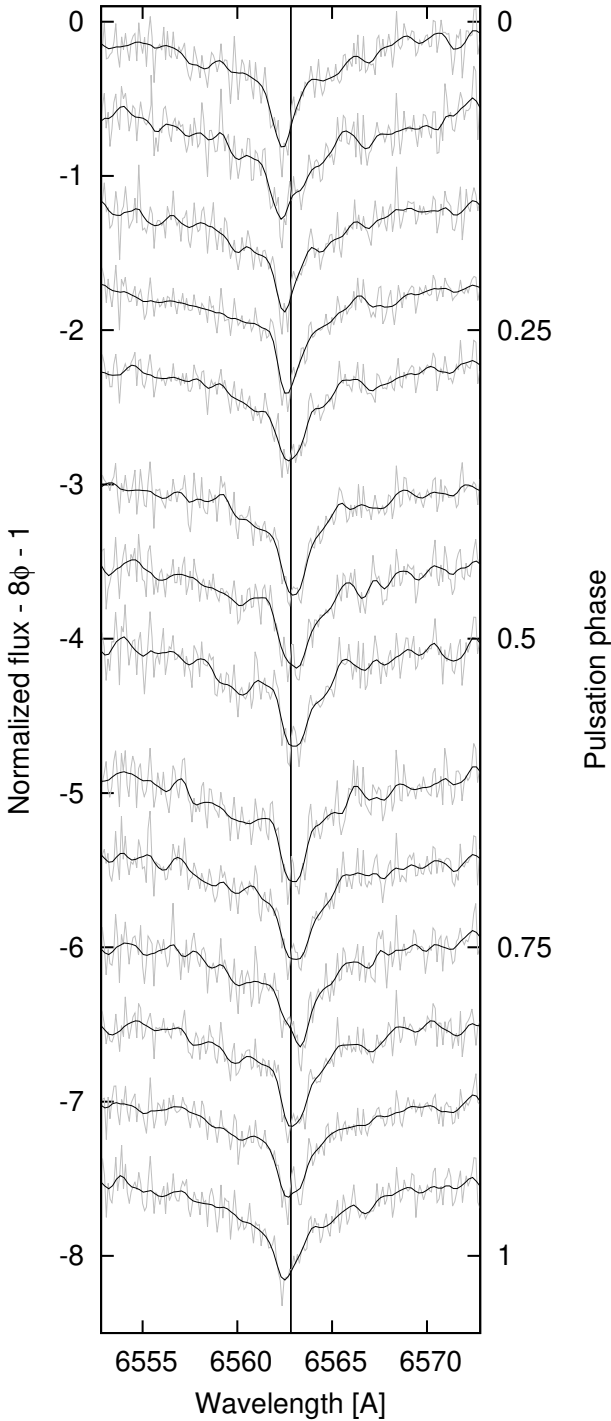


**Figure 5.**  $H\alpha$  line variations of T Sex over the pulsation cycle in the stellar rest frame. The normalised spectra are shown with thin grey line. The black curves are the smoothed spectra. Vertical line marks the laboratory position of the  $H\alpha$  line.

one. Such line-profile variations has not been reported for RRc stars before.

This line asymmetry is a remarkable difference compared to the variation of the  $H\alpha$  line of RR Lyrae. In that case, an  $H\alpha$  line doubling can be detected between  $\phi = 0.943$  and  $\phi = 1.027$  but the core of the line remains symmetric in all phases (Gillet et al.

2019). Additionally, some metallic lines of RR Lyrae also show phase-dependent profile distortions around the brightness maxima ( $\phi \sim 0.91 - 0.97$ ) and the strength of this effect depends on the Blazhko phase (Chadid & Gillet 1996, 1997). These two phenomena have been explained by the same physical mechanism: a hydrodynamical shock wave passing through the pulsating atmosphere causing two distinct absorbent layers (Schwarzschild 1952; Fokin & Gillet 1997). In this case, the asymmetric metallic lines would be nothing more than overlapping double lines.

The  $H\alpha$  line doubling and the asymmetry of metallic lines in R Rab stars appear only around the phase of maximum brightness. The phenomenon presented here is more similar to that observed in some metallic lines of classical Cepheids and  $\beta$  Cep stars (Nardetto et al. 2008, 2013). Nardetto et al. (2008) discussed three explanations for the effect. The time- and wavelength dependence of the limb-darkening within the spectral lines, velocity gradients in the atmosphere and the relative motion of the line-forming region with respect to the corresponding mass elements. The third explanation is closely related to the one that was mentioned for RRabs. Nardetto et al. (2008) concluded that for quantitative modelling of line asymmetries, a detailed hydrodynamic model, in which convection is taken into account, should be combined with a wavelength-dependent radiative code.

### 5.2.1 Phenomenologic explanation

Pulsating atmospheric models that take into account both convection and shock waves and are able to compute synthetic lines profiles for Cepheids or RR Lyrae stars have not yet been developed. There is, however, a smart tool, called NRP ANIMATION CREATOR (NRPAC)<sup>3</sup> (Schrijvers et al. 1997; Telting & Schrijvers 1997; Schrijvers & Telting 1999) that allows us to model line profile variations of pulsating stars. The program is optimised for fast rotating non-radially oscillating variables, such as  $\delta$  Scutis and related stars. Because of its assumptions (e.g. of adiabatic pulsation) it is not suitable for quantitative analysis of line-profile variations in an RR Lyr pulsator. Nonetheless, if we assume a radially pulsating ( $l = m = 0$ ) star with the parameters of a typical RRc star (mass  $M = 0.65 M_{\odot}$ , radius  $R = 4 R_{\odot}$ , 3D velocity amplitude  $A(v) = 20 \text{ km s}^{-1}$ , pulsation frequency  $f_1 = 0.3 \text{ d}^{-1}$ ,  $v \sin i = 15 \text{ km s}^{-1}$ ), we can qualitatively reproduce the observed line-profile distortions.

Fig. 7 shows the line profile of two extreme phases (the maximal contraction in the left side, and the maximal expansion in the right) of a radially pulsating star. The line profiles of the resting stars are shown by thin lines. The same parameters were used for all the plots, except for  $v \sin i$ . We used  $v \sin i = 1 \text{ km s}^{-1}$  for the top row and  $15 \text{ km s}^{-1}$  for the bottom row. For  $v \sin i = 1 \text{ km s}^{-1}$ , the line profile is practically not distorted and it shows similar profiles as the observed one of Gillet et al. (2019) for RR Lyrae. Fig. 7 illustrates well that the key of qualitatively reproducing the observed line-profile variations of T Sex is applying a relatively high  $v \sin i$  value in NRPAC.

Preston et al. (2019) summarises the present knowledge of RR Lyrae axial rotation and macroturbulence, which are generally hard to separate because these two phenomena broaden the line profiles in a similar fashion. Preston et al. (2019) found an upper limit for the macroturbulent velocity of RRab stars as  $5 \pm 1 \text{ km s}^{-1}$ . They also showed that this velocity is less uniform for RRc stars and it could be as high as  $\sim 12 \text{ km s}^{-1}$ .

<sup>3</sup> <http://staff.not.iac.es/~jht/science/nrpform/>

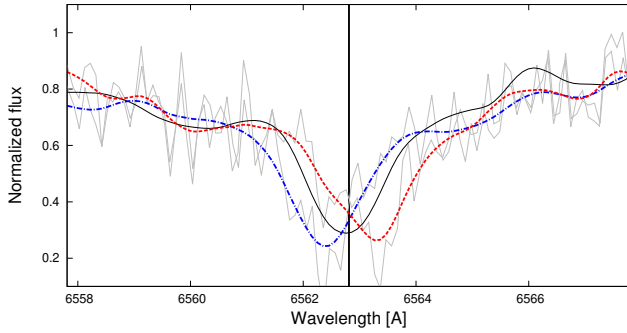


**Figure 6.**  $H\alpha$  line-profile distortions of T Sex over the pulsation cycle. The normalised spectra are shown with thin grey lines. The black continuous curve shows a smoothed spectrum at  $\phi = 0.607$  with symmetric line profile corrected with its relative velocity ( $9.39 \text{ km s}^{-1}$ ) to the stellar rest frame. The blue dash-dotted curve is a blue shifted asymmetric spectrum at  $\phi = 0.003$  while the red dashed curve shows the red shifted asymmetric spectrum at  $\phi = 0.737$ . The vertical line indicates the laboratory position of the  $H\alpha$  line.

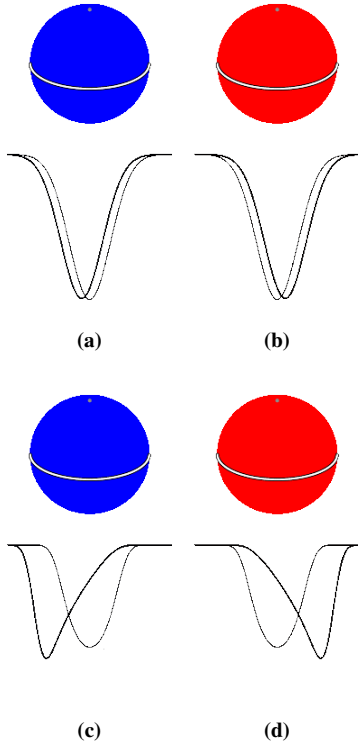


**Figure 7.** Extreme cases of line profile variation on a radially pulsating star with the parameters of a typical RRc stars. The figures were prepared by using NRP Animation Creator. The subfigures a) and c) show maximal contraction b) and d) maximal expansion phases. In the top row  $v \sin i = 1 \text{ km s}^{-1}$ , in the bottom row  $v \sin i = 15 \text{ km s}^{-1}$ .

As we have seen, reproducing the line-profile variations of T Sex with NRPAC requires a sufficiently large  $v \sin i$ . This tool, however, does not use the macroturbulent velocity as a free parameter, therefore the suggested high  $v \sin i$  does not necessarily mean a high equatorial rotation speed, but could imply a more intense macroturbulence caused by the convection. This finding agrees with the theoretical calculations of Gautschi (2019), showing the more significant role of atmospheric convection in RRc stars than in RRab stars. It means, on the one hand, that convection is more important in the energy transport and, on the other hand, that, unlike RRab stars, it is present in almost all pulsation phases.

The question may arise whether the non-radial mode discussed in Sec. 3 could cause the observed line profile changes or not. Most probably not. First, the expected period of an  $l = 8$  non-radial is  $P_3 = 1/f^{(3)} = 0.41808 \text{ d}$  significantly different from the pulsation period, which is the period of the observed effect. Second, non-radial modes primarily modify the shape of line cores, while only slightly shift the position of the lines (see e.g. Telting 2003 and references therein). However, we see strong shifts in the line position: there is a difference of  $\sim 1 \text{ Å}$  between the two extreme positions of the  $H\alpha$  line in Fig 6, which is typical for a radial mode. Thirdly, the degree of line distortion expected from an  $l = 8$  mode is much smaller than that results from the large macroturbulence discussed above. If we prepare simulated line profiles by NRCAP assuming a combination of a radial ( $l = 0$ ) and an  $l = 8$  non-radial modes, the obtained simulated line profiles are indistinguishable from those shown in Fig. 7. If we could subtract the variations of the radial mode, and examine only the effects of non-radial mode, our simulated line profiles show that even then we obtain a measurable (some percents of) variation only under some special circumstances, when the inclination is high and the absolute value of the sectorial number  $|m|$  is also high. In summary, the shape, strength, and period of the line profile variations found do not support the explanation that this would be caused by a non-radial mode.

### 5.2.2 Spectral fitting

We also performed a more quantitative estimation for macroturbulent velocity by fitting theoretical stellar model atmospheres to the observed spectra. Following Sneden et al. (2017), we prepared a good S/N combined spectrum from the best 16 spectra, which samples the complete pulsation cycle almost evenly. Then we shifted each of them with the corresponding radial velocity and computed the median spectrum. The vicinity of the Mg triplet (between 5165 and 5190 Å) of the median spectrum is shown in Fig. 8 with black dots. We fitted theoretical spectra between 5150 and 5190 Å to this median spectrum by minimizing  $\chi^2$ .

We calculated the atmospheric parameters of T Sex from this region using the ‘Synthetic spectral fitting’ tool of iSPEC. After trying several radiative transfer codes (SPECTRUM, Turbospectrum, MOOG) integrated into the iSPEC package, we concluded that there is no significant difference in the obtained fits in our case, so the integrated SPECTRUM radiative transfer code (Gray & Corbally 1994) and MARCS GES model atmospheres (Gustafsson et al. 2008) were selected. The solar abundance of Grevesse et al. (2007) and GES (Gaia-ESO Survey) atomic line list (Heiter et al. 2015) were used.

Several test runs showed that the parameters of Sneden et al. (2017) obtained from the phase-averaged spectrum agrees within the errors with the results from our median spectrum, therefore, we accepted and updated them. We accepted  $T_{\text{eff}} = 6960 \pm 160 \text{ K}$  effective temperature,  $\log g = 2.12 \pm 0.16$ ,  $[M/\text{Fe}] = -1.48 \pm 0.1$  metallicity and  $[\alpha/\text{Fe}] = 0.51 \pm 0.18$  alpha-element enhancement.



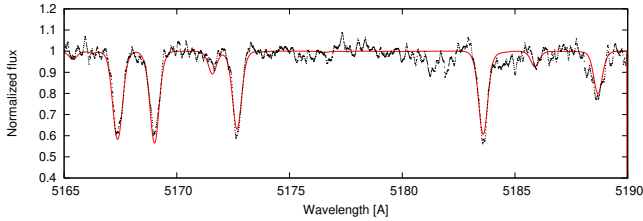


**Figure 8.** Spectral fit for the Mg triplet range of T Sex. The small black dots show the median spectrum over the whole pulsation cycle. The red continuous line shows the best-fitting synthetic spectrum.

However, we use our higher value for the microturbulence ( $\xi = 3.8 \text{ km s}^{-1}$ ) because it always resulted in better spectral fits than  $\xi = 2.3 \pm 0.16 \text{ km s}^{-1}$  of Sneden et al. (2017). Note that the errors correspond to one  $\sigma$  uncertainties.

The macroturbulence  $v_{\text{mac}}$  and the projected rotational velocity  $v \sin i$  lead to similar line broadening effects, as Preston et al. (2019) showed, and it is difficult to separate them. We arrived at the same conclusion here. A similarly accurate fit can be achieved either with  $v \sin i = 0$ ,  $v_{\text{mac}} = 23 \text{ km s}^{-1}$  or with  $v \sin i = 15$ ,  $v_{\text{mac}} = 0 \text{ km s}^{-1}$ , respectively. Since RR Lyrae stars are slow rotators, it is very likely that the first case is closer to reality. This fit is shown by a red line in Fig. 8.

Although in a completely different way, we arrived at the same conclusion as before by studying the variations in the  $H\alpha$  line: either  $v \sin i$  or rather  $v_{\text{mac}}$  is relatively large ( $\sim 15\text{--}20 \text{ km s}^{-1}$ ). This supports our phenomenological explanation of the periodic line distortions.

### 5.3 Sodium lines

#### 5.3.1 Line doubling

We show the Na I D line-profile variations of T Sex over the pulsation cycle in Fig. 9. In the left panel the spectra are plotted in a system co-moving with the pulsation, that is, the instantaneous radial velocity was subtracted from each spectrum. In other words, this system moves with the average pulsation motion of the atmosphere defined by the radial velocity curve in Fig. 4. It can be seen that the D<sub>1</sub> and D<sub>2</sub> line profiles are rather similar in all phases: they show significant deviation from a single Gaussian profile between the phases of  $\phi \approx 0.28$  and  $\phi \approx 0.88$ . The distortion becomes line doubling between  $\phi \approx 0.37$  and  $\phi \approx 0.80$ . The phenomenon is observable over 60% of the pulsation cycle.

Line doubling of the sodium D lines in the spectrum of a fundamental-mode pulsating RRab star (RR Lyr itself) was reported for the first time by Gillet et al. (2017), who found this line doubling to be coincident with an  $H\alpha$  emission of RR Lyr at the phase  $\phi \approx 0.227$ . In a more recent and detailed study, Gillet et al. (2019) showed that the D<sub>1</sub> line is doubled over 75% of the pulsation cycle. The position of the redder component is fixed during the whole pulsation cycle within the stellar rest frame, therefore this component was explained by interstellar origin.

Our present study shows line doubling phenomenon in an over-tone pulsating RRc star. As we see in the left-hand panel of Fig. 9, the position of the red part of the line is fixed with respect to the co-moving frame, that is, it follows the atmospheric motions, which are represented by the radial velocity curve and obtained from the averaged motions of metallic lines. Thus, it can be assumed that the

atmospheric layer where this line is formed is at or near the layer where the metallic lines taken into account in the calculation of the radial velocity curve are formed.

The position of the blue component in the left panel of Fig. 9 varies with the phase but this is a virtual variation. When we construct the spectral variations over the pulsation cycle within a rest of frame of the center-of-mass of T Sex (right panel of Fig. 9), we see that actually the position of the blue component is fixed. In other words this component does not share the motion of the pulsating atmosphere.

What is the origin of these ‘fixed’ components? The telluric origin is unlikely because the known telluric absorption lines in this spectral region (see e.g. Hobbs 1978) are weak and they have complex fine structure which has not been detected. Circumstellar and interstellar origin are the two natural potential explanations. According to Gillet et al. (2019), the  $+50.3 \text{ km/s}$  velocity interstellar line they found in the spectra of RR Lyr may originate from the wall of the Local Bubble (Frisch et al. 2011). This explanation applies for our case as well. The recent 3D-map of the interstellar gas based on Na (and Ca) absorption observations (Vergely et al. 2010; Welsh et al. 2010) shows a gas cloud toward the direction of T Sex ( $l = 235^\circ 38'$ ,  $b = +40^\circ 36'$ ). This cloud is also part of the material that forms the wall of the Local Bubble. Although the map includes only the 300 pc neighbourhood of the Sun, the contribution of more distant matter to the interstellar absorption is likely to be small, since T Sex have a high Galactic latitude, where we do not expect significant interstellar matter so far away.

Distinguishing between circumstellar and interstellar material is generally an observing task. We have to observe several stars that are close to the target star in space, and if we observe similar interstellar absorption in the check stars, we can conclude that these lines originate from the interstellar space. Otherwise, if only the target shows these lines, that suggests a circumstellar origin. The method was successfully applied for discovering circumstellar discs (see e.g. Redfield 2007; Redfield et al. 2007; Rebollido et al. 2018). In the case of distant sources beyond the Local Bubble, the picture could be more complicated. As Points et al. (2004) showed, each selected star of the  $\chi$  and h Per double cluster show different Na I D absorption properties. This reflects the fine structure of the interstellar material in the line of sight. The distance of T Sex ( $803 \pm 40 \text{ pc}$ , from the Gaia DR2 Gaia Collaboration 2016, 2018) is much larger than the wall of the Local Bubble ( $\sim 100\text{--}200 \text{ pc}$ ), but, due to its high galactic latitude ( $l = +40^\circ$ ), no significant interstellar material is expected beyond the Local Bubble.

In the February of 2020, we observed 5–5 spectra of two brighter stars (HD 85879 and HD 85817) appearing close to the celestial position of T Sex, to investigate the issue. We determined their radial velocities with the same method as we described for T Sex in Sect. 4. The obtained values are  $16.01 \pm 0.34 \text{ km s}^{-1}$  and  $29.19 \pm 0.37 \text{ km s}^{-1}$  for HD 85879 and HD 85817, respectively. Both values are in agreement with the Gaia results (Gaia Collaboration 2018).

We selected five spectra for T Sex from those phases where there is no line doubling (between  $\phi = 0.87$  and  $0.14$ ), i.e. the fixed components of the Na lines coincide with the moving components. The shift value  $31.7 - 13.2 = 18.5 \text{ km s}^{-1}$  obtained from Fig. 9 meaning the barycentric velocity of the (interstellar) component was also applied for all three spectra. After averaging the 4–4 best S/N spectra for all three stars, the result is plotted in Fig. 10.

The wide line profiles of HD 85817 (top blue curve) do not show line doubling, only on the red wing of both lines of Na D doublet slight breaks can be suspected just in the proper posi-

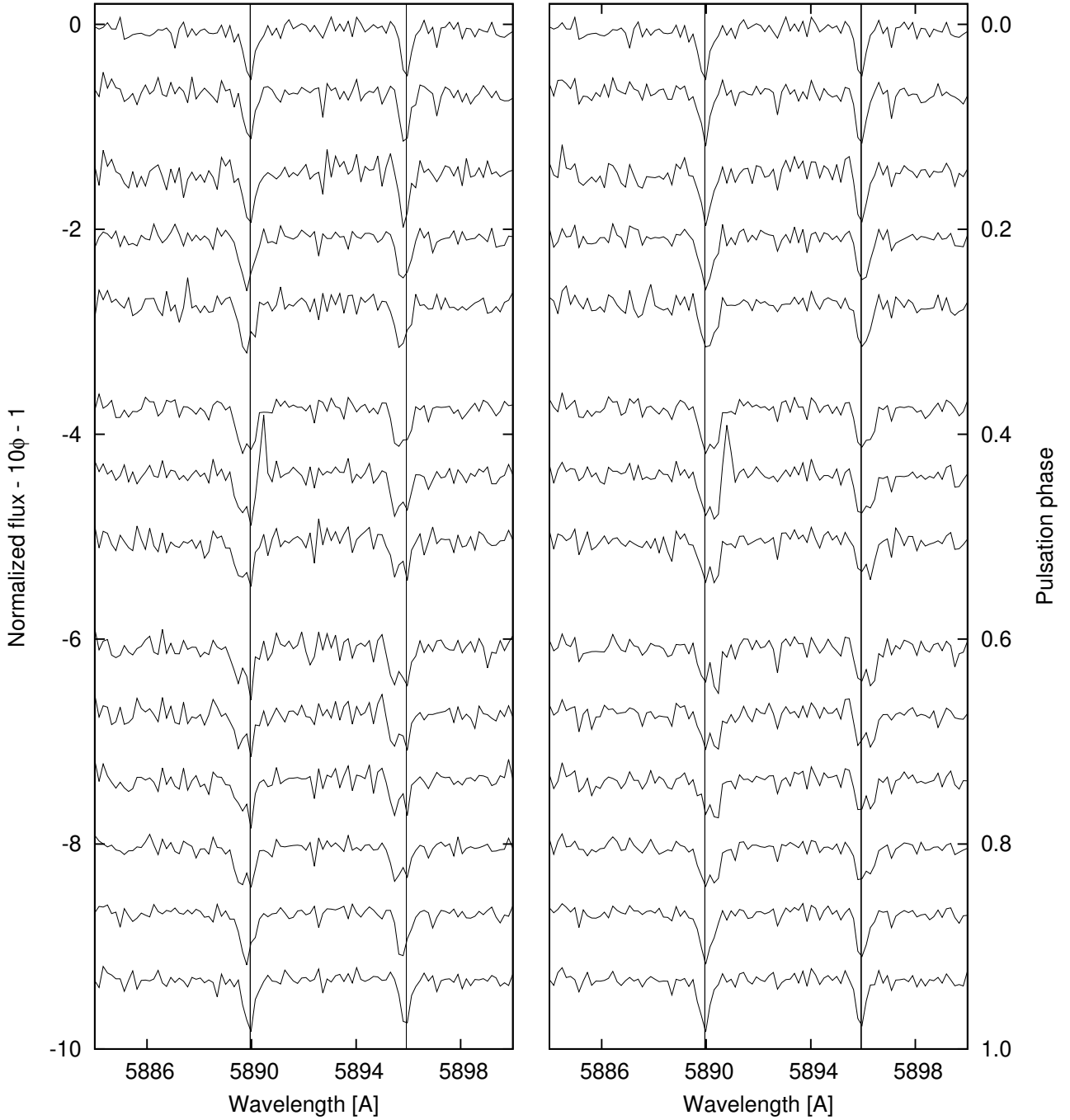


**Figure 9.** Sodium line variations of T Sex over the pulsation cycle in a system co-moving with the pulsating atmosphere (in the left) and in the stellar centre-of-mass rest frame (in the right), respectively. The smoothed and normalised spectra are shifted vertically according to the pulsation phase. The thin vertical lines indicate the laboratory wavelengths of the Na D<sub>1</sub> and D<sub>2</sub> lines. Spectra in the right-hand panel are shifted with the radial velocity of the stellar centre-of-mass ( $-13.2 \text{ km s}^{-1}$ ) to transform the Na D lines to the vicinity of their laboratory wavelengths. The slightly different line shapes are due to differences in the spline interpolation.

tion. These asymmetric profiles might be the result of a blend between the star and interstellar lines. Unfortunately, the radial velocity difference between HD 85879 and the interstellar matter is small ( $\sim 2.5 \text{ km s}^{-1}$ ), therefore, the lines coming from the star and from the interstellar material can not be distinguished (bottom black curve). Although these control measurements did not provide a definite answer to the question, they rather support, in particular those

of HD 85817, that we are dealing here with material of interstellar and not circumstellar origin.

### 5.3.2 *P Cyg profile?*

At the phase  $\phi = 0.438$  T Sex shows an emission peak redwards to the red component of Na D<sub>2</sub> line (see Fig. 9) and it forms a P Cyg



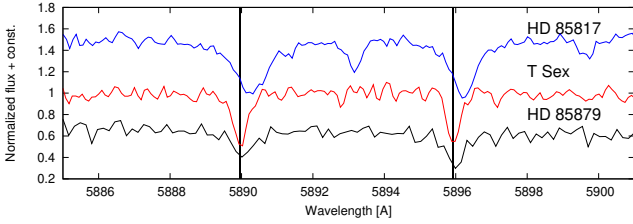


**Figure 10.** Spectra around the Na D lines of T Sex and two neighbouring stars; HD 85879 and HD 85817. In each case, five individual spectra were combined and equal shifts (with  $18.5 \text{ km s}^{-1}$ ) were applied to transform the wavelengths of the Na lines to the laboratory values.

profile with the absorption line. As we have seen above this redder line component comes from the stellar photosphere. Appearance of sodium emission is remarkable because such phenomenon has not been reported for any RR Lyrae star before.

We investigated possible sources of this spectral feature. The first possibility to exclude was an observational or reduction error. This emission line profile is constructed by 6 data points which means that the spectral resolution is much higher than the line width. Therefore, it is highly unlikely that the line would be an incorrectly treated cosmic. Perhaps a more spacious anomaly in the CCD frame could cause this. However, as we checked it, no such discrepancies (e.g. hot column, scattered light, saturation trail) are seen in the raw observed frame. Additionally, there is no extra flux in any of the orders below and above the order which shows the line.

It is possible that the a given emission line does not come from the stars, but somewhere from the Earth's atmosphere. The peak intensity of our  $\lambda 5890$  line is  $\sim 72$  per-cents higher than the strongest known optical telluric emission line of O I at  $\lambda 5577$ . The intensity of telluric sodium D<sub>2</sub> line is much weaker 5 per-cents of this atmospheric O I emission line (Louistisserand et al. 1987). Furthermore, in the case of terrestrial origin, the phenomenon should be detected more or less continuously. These arguments make instrumental or terrestrial origin very unlikely.

Emission of a metallic line for RR Lyr stars has been completely unknown so far. H $\alpha$  emission is known for three phase intervals of RRab stars. The H $\alpha$  emission just before the luminosity maximum ( $\phi \sim 0.89 - 0.93$ ) was detected long ago (Struve & Blaauw 1948; Stanford 1949). Later, Gillet & Crowe (1988) found a blue emission shoulder of the H $\alpha$  line. This emission appears around  $\phi \sim 0.73$ , which is the position of the ‘bump’ near the photometric minimum. The third emission effect, a red emission shoulder around  $\phi \sim 0.18 - 0.39$  was discovered by Preston (2011).

Beyond the hydrogen emission phases of RRab stars, helium emissions were also discovered by Preston (2009) in a sample of 11 observed RRab stars. A stronger emission of He I D<sub>3</sub> line at  $\lambda 5875.66$  and a weaker emission at  $\lambda 6678.16$  were observed in all sample stars during rising light. A further helium emission of He II at  $\lambda 4685.68$  was also reported by Preston (2011).

For all of these cases, the physical explanation of the emission is similar: different shock waves in the atmosphere (see Gillet & Fokin 2014 and references therein). But similarly to the observations, the theoretical efforts have also been concentrated on fundamental-mode pulsating RRab stars. We were not able to find any theoretical study that investigates shock properties in RRC stars. Maybe the reason is that because of the smaller atmospheric velocities of RRC stars, no strong shocks are expected. From an observa-

tional point of view, Sneden et al. (2017) found no signs of shocks (line doubling, emission) in the spectra of 7 RRC stars, and estimated an upper limit of  $\sim 10 \text{ km s}^{-1}$  for any possible atmospheric shocks. At the same time, the authors discussed the possibility of a compression wave around  $\phi \sim 0.52 \pm 0.05$  where certain H $\alpha$  radial-velocity curves show a secondary maximum. As they mentioned, this wave would be “qualitatively similar to the shock Sh<sub>PM3</sub> of RRab stars (Chadid et al. 2014), which produces compression heating during infall.”

If we look into Gautschy’s latest theoretical calculations (see fig. 4 in Gautschy 2019) phase  $\phi \sim 0.4 - 0.5^4$  of RRC stars corresponds to the phase where the early shock appears in the RRab stars (Hill 1972). Namely, where the luminosity functions of the cool edge and the hot edge of the He II partially ionised zones intersect. The physical meaning of this intersection is the collision between the infalling high atmosphere and the slower shrinking photosphere.

Based on these, our finding of Na emission in the appropriate pulsation phase both agrees with the theoretical calculations and the preliminary observational expectations. The wavelength difference between the absorption and emission components of D<sub>2</sub> line is  $0.46 \text{ \AA}$ , giving a velocity difference of  $23.4 \text{ km s}^{-1}$ . Sodium absorption lines, along with other metallic lines, are formed practically in the photosphere. The velocity of the photosphere at this phase is  $5.8 \text{ km s}^{-1}$ . The total velocity of the supposed compression wave in the stellar rest frame is  $29.2 \text{ km s}^{-1}$ . This is almost an order of magnitude smaller than the shock wave velocities estimated for RRab stars.

Our detection of this emission rises two questions. First, why did not we observe similar emission at line D<sub>1</sub>? And second, why did not Sneden et al. (2017) detect it in their very good time-sampled spectra? There might be an answer to the first question: the intensity ratio between Na emission D<sub>1</sub> and D<sub>2</sub> lines can be strongly varying between  $0.5 - 0.9$  depending on the physical condition of the emitting material (e.g. Nikaidou & Kawaguchi 1983; Slanger et al. 2005). The explanation of the second question may be that the phenomenon is temporary. This would not be unprecedented, since the cycle-to-cycle variation of RR Lyrae spectra is a known phenomenon (Chadid 2000). For more definite answers, we need more spectroscopic time series observations.

## 6 SUMMARY

In this paper, we presented our results based on new photometric and spectroscopic time series on one of the brightest RRC star, T Sex. Our main findings are:

- We found from the Fourier analysis of the photometric data set of the *TESS* space telescope that the light curve of T Sex can be described by two independent frequencies: the frequency of the radial overtone pulsation,  $f_1$ , and a frequency belonging most probably to an  $l = 8$  non-radial pulsation mode. The speciality of the Fourier spectrum of T Sex is that the usual  $f_x$  frequency is not significant, only  $0.5f_x$  is observed. No similar stars have been reported before by space photometry. Such stars are also very rare in ground-based observations (seven stars among 960,  $\sim 0.7\%$ , Netzel & Smolec 2019).

<sup>4</sup> We mention that Gautschy denotes the maximum radius by phase  $\varphi = 0.0 = 1.0$  and not the maximum brightness as we use here. There is a  $\sim 0.68$  phase shift between the two zero-points.

- Based on our time-resolved spectroscopic measurements, we showed a characteristic phase-dependent periodic distortion of the H $\alpha$  line. This type of line-profile variation is significantly different from RRab stars, e.g., from the almost unchanging profiles seen at RR Lyr (Gillet et al. 2019). This type of line-profile changes have not previously been published for RR Lyrae stars, only for other radial pulsators (Nardetto et al. 2008, 2013). The phenomenon is most likely caused by the relatively high macroturbulent velocity of T Sex ( $\sim 15\text{--}20\text{ km s}^{-1}$ ), which can be caused by convection. This plays a more important role in the pulsation of RRc stars than in RRab pulsators.

- We discovered a phase-dependent line doubling of the Na D lines. This is the first case that such line doubling has been reported for overtone pulsating RR Lyrae stars. The possible explanation of the feature is the same as in the case of RR Lyr (Gillet et al. 2019): one of the line components come from the star, while the other one originates from the interstellar medium. This finding calls the attention to the fact that the characteristic velocities of the atmosphere of an RR Lyrae star during pulsation is similar to the velocity of the ISM clouds in the wall of the Local Bubble. Thus, it is expected that most Galactic field RR Lyr stars will show similar Na D line doubling.

- At the phase  $\phi = 0.438$ , a definite emission peak was found on the red side of the sodium D<sub>2</sub> line, which forms a P Cyg profile with the absorption component. The appearance of P Cyg profiles in RR Lyrae spectra is usually associated with shock waves. Although no strong shock waves are expected for RRc stars, the appropriate phase of the detected event and the calculated shock wave velocity ( $\sim 30\text{ km s}^{-1}$ ) also suggest the appearance of a weak shock wave. Due to the single detection, the intrinsic nature of the phenomenon must be verified in the future.

## ACKNOWLEDGEMENTS

This work was supported by the Hungarian National Research, Development and Innovation Office by the Grant NN-129075 and the Lendület Program of the Hungarian Academy of Sciences, project No. LP2018-7/2018. JMB thanks to Dr A. Moór and Dr R. Szabó for their valuable suggestions.

This work has made use of data from the European Space Agency (ESA) mission *Gaia* (<https://www.cosmos.esa.int/gaia>), processed by the *Gaia* Data Processing and Analysis Consortium (DPAC, <https://www.cosmos.esa.int/web/gaia/dpac/consortium>). Funding for the DPAC has been provided by national institutions, in particular the institutions participating in the *Gaia* Multilateral Agreement.

## DATA AVAILABILITY

The raw and processed spectroscopic data underlying this article will be shared on reasonable request to the corresponding author. The radial velocity data obtained from the spectra are available in the online supplementary material under the name of `tsex_vrad.dat`. The photometric data underlying this article were accessed either from ASAS-3 database <http://www.astrouw.edu.pl/asas/?page=aasc&catsrc=asas3> and from Mikulski Archive for Space Telescopes <https://mast.stsci.edu/portal/Mashup/Clients/Mast/Portal.html> (TESS). The derived data generated in this research will be shared on reasonable request to the corresponding author.

## REFERENCES

- Barnes, T. G., Moffett, T. J., Hawley, S. L., Slovak, M. H., Frueh, M. L. 1988, *ApJS*, 67, 403
- Benkő, J. M., Jurcsik, J., Derekas, A. 2019, *MNRAS*, 485, 5897
- Blanco-Cuaresma, S. 2019, *MNRAS*, 486, 2075
- Blanco-Cuaresma, S., Soubiran, C., Heiter, U., Jofré, P. 2014, *A&A*, A111
- Chadid, M. 2000, *A&A*, 359, 991
- Chadid, M., Gillet, D. 1996, *A&A*, 308, 481
- Chadid, M., Gillet, D. 1997, *A&A*, 319, 154
- Chadid, M., Sneden, C., Preston, G. W. 2017, *ApJ*, 835, id.187
- Chadid, M. et al. 2014, *AJ*, 148, id.88
- Derekas, A. et al. 2017, *MNRAS*, 464, 1553
- Dziembowski, W. A. 2016, in *RRL2015 – High-Precision Studies of RR Lyrae Stars*, eds. L. Szabados, R. Szabó, K. Kinemuchi, *Comm. Konkoly Obs.*, 105, pp. 23–30.
- Fokin, A. B., Gillet, D. 1997, *A&A*, 325, 1013
- Frisch, P. C., Redfield, S., Slavin, J. D. 2011, *ARA&A*, 49, 237
- Gaia Collaboration 2016, *A&A*, 595, A1
- Gaia Collaboration 2018, *A&A*, 616, A1
- Gautschi A. 2019, *Astro-ph*:1909.10444
- Gillet, D., Crowe, R. A. 1988, *A&A*, 199, 242
- Gillet, D., Fokin, A. B. 2014, *A&A*, 565, A73
- Gillet, D., et al. 2017, *A&A*, 607, A51
- Gillet, D., et al. 2019, *A&A*, 623, A109
- Gontcharov, G. A. 2006, *Astron. Letters*, 32, 759
- Gray, R. O., Corbally, C. J. 1994, *AJ*, 107, 742
- Grevesse, N., Asplund, M., Sauval, A. J. 2007, *Space Sci. Rev.*, 130, 105
- Gruberbauer, M. et al. 2007, *MNRAS*, 379, 1498
- Gustafsson, B., Edvardsson, B., Eriksson, K., Jørgensen, U. G., Nordlund, Å., Plez, B. 2008, *A&A*, 486, 951
- Heiter, U. et al. 2015, *A&A*, 582, A49
- Hill, S. J. 1972, *ApJ*, 178, 793
- Hobbs, L. M. 1978, *ApJ*, 222, 491
- Jurcsik, J. et al. 2015, *ApJS*, 219, 25
- Jurcsik, J. et al. 2017, *MNRAS*, 468, 1317
- Karp, A. H. 1975, *ApJ*, 201, 641
- Kollmeier, J. A. et al. 2013, *ApJ*, 775, id.57
- Lenz, P., Breger, M. 2005, *CoAst*, 146, 53
- Le Borgne, J. F. et al. 2007, *A&A*, 476, 307
- Liu, T., Janes, K. A. 1989, *ApJS*, 69, 593
- Louistisserand, S., Büchner, A., Koutchmy, S., Lamy, Ph. 1987, *A&AS*, 68, 539
- Maintz, G. 2005, *A&A*, 442, 381
- Molnár, L. et al. 2015, *MNRAS*, 452, 4283
- Moskalik, P. 2013, in *Stellar Pulsations: Impact of New Instrumentation and New Insights*, eds: J. C. Suárez, R. Garrido, L. A. Balona & J. Christensen-Dalsgaard, *Astrophys. Space Sci. Proc.* 31, p. 103
- Moskalik, P. et al. 2015, *MNRAS*, 447, 2348
- Nardetto, N. et al. 2008, *A&A*, 489, 1235
- Nardetto, N. et al. 2013, *A&A*, 553, A112
- Netzel, H., Smolec, R. 2019, *MNRAS*, 487, 5584
- Netzel, H., Smolec, R., Dziembowski, W. 2015, *MNRAS*, 451, L25
- Nikaidou, Y., Kawaguchi, I. 1983, *Sol. Phys.*, 84, 49
- Olech, A., Moskalik, P. 2009, *A&A*, 494, L17
- Points, S. D., Lauroesch, J. T., Meyer, D. M. 2004, *PASP*, 116, 801
- Pojmański, G., Pilecki, B., Szczygieł, D. 2005, *Acta Astron.* 55, 275.
- Preston, G. W. 2009, *A&A*, 507, 1621
- Preston, G. W. 2011, *AJ*, 141, id.6
- Preston, G. W., Paczyński, B. 1964, *ApJ*, 140, 181
- Preston, G. W., Sneden, C., Chadid, M., Thompson, I. B., Shtetman, S. A. 2019, *AJ*, 157, id.153
- Prudil Z., Smolec R., Skarka M., Netzel H. 2017, *MNRAS*, 465, 4074
- Rebolledo, I. et al. 2018, *A&A*, 614, A3
- Redfield, S. 2007, *ApJ*, 656, L97
- Redfield, S., Kessler-Silacci, J. E., Cieza, L. A. 2007, *ApJ*, 661, 944
- Ricker, G. R. et al. 2015, *J. Astron. Tel. Instr. Sys.*, 1, id.014003

- Rudolf, N., Günther, H. M., Schneider, P. C., Schmitt, J. H. M. M. 2016, *A&A*, 585, A113
- Schrijvers, C., Telting, J. H., Aerts, C., Ruymaekers, E., Henrichs, H. F. 1997, *A&AS*, 121, 343
- Schrijvers, C., Telting, J. H. 1999, *A&A*, 342, 453
- Schwarzschild, M. 1952, *Transactions of the IAU VIII*, ed., P. TH. Oosterhoff (Cambridge: Cambridge University Press), 8, 811
- Slanger, T. G. et al. 2005, *J. Geophys. Res.*, 110, D23302
- Snedden, C., Preston, G. W., Chadid, M., Adamów, M. 2017, *ApJ*, 848, id.68
- Sódor, Á., Skarka, M., Liška, J., Bognár, Zs. 2017, *MNRAS*, 465, L1
- Stanford, R. F. 1949, *ApJ*, 109, 208
- Struve, O., Blaauw, A. 1948, *ApJ*, 108, 60
- Szabó, R. et al. 2014, *A&A*, 570, A100
- Tift, W. G., Smith, H. J. 1958, *ApJ*, 127, 591
- Telting, J. H. 2003, *Ap&SS*, 284, 85
- Telting, J. H., Schrijvers, C. 1997, *A&A*, 317, 723
- Tody, D. 1986, in *Proc. SPIE Instrumentation in Astronomy VI*, ed. D. L. Crawford, p. 627
- Tody, D. 1993, in *Astronomical Data Analysis Software and Systems II*, eds. R. J. Hanisch, R. J. V. Brissenden, & J. Barnes, *ASP Conference Ser.*, Vol 52, p. 173
- Vergely, J.-L., Valette, B., Lallement, R., Raimond, S. 2010, *A&A*, 518, A31
- Welsh, B. Y., Lallement, R., Vergely, J.-L., Raimond, S. 2010, *A&A*, 510, A54

This paper has been typeset from a  $\text{\TeX}/\text{\LaTeX}$  file prepared by the author.